


Morphological characteristics of carboxymethylated cellulose nanofibrils: the effect of carboxyl content

Wanhee Im · Araz Rajabi Abhari · Hye Jung Youn · Hak Lae Lee 

Received: 13 June 2018 / Accepted: 10 August 2018 / Published online: 16 August 2018
© Springer Nature B.V. 2018

Abstract This study investigated the effects of carboxyl content and mechanical treatment intensity on the morphological characteristics of carboxymethylated cellulose nanofibrils (CM CNFs) and on the rheological properties of CM CNF suspension. The mechanical properties of self-standing CM CNF film were also examined. CM CNFs produced under different conditions had similar, uniform widths of about 5 nm, as measured using transmission electron microscope images and Image J software. The aspect ratios of three CM CNFs were evaluated using gel point analysis and the crowding number theory. Higher carboxyl content in the CM CNFs reduced the amount of mechanical energy required and increased the aspect ratio. The rheological properties and the tensile properties of CNF film were all strongly influenced by the aspect ratio of the CM CNFs. The CM CNF samples with higher aspect ratios produced stronger suspension network structures and had greater tensile properties.

Keywords Cellulose nanofibrils · Aspect ratio · Gel point · Carboxymethylation · Carboxyl content

Introduction

Recently, cellulose nanofibrils (CNFs) have been the subject of extensive scientific research. Many studies have used CNFs as a reinforcing material in various nanocomposites (Liu et al. 2013; Errezma et al. 2017; Yao et al. 2017). CNFs are suitable reinforcing materials for nanocomposites because of their inherent characteristics such as biodegradability, renewability, very high tensile strength, low thermal coefficient, etc. (Fujisawa et al. 2013; Saito et al. 2013).

However, several challenges limit the use of CNFs in commercial applications. One of the most important challenges associated with nano-fibrillation of CNF is the high-energy consumption required by fibrillating processes (Isogai 2018). Mechanical, enzymatic, and chemical pretreatments have been tested as methods to facilitate nanofibrillation (Wang et al. 2015; Ko et al. 2011; Suflet et al. 2006), which made the CNF a more attractive material for commercial applications (Nechporchuk et al. 2016). Among these pretreatment methods, chemical pretreatments that introduce charged groups to the CNF surface have made it possible to obtain CNFs with narrow width distributions (Saito et al. 2006; Wågberg et al. 2008). These charged groups also provide electrostatic repulsion between the fibrils, which creates the well-dispersed CNF suspensions that are necessary to form final products that have the uniform and mechanical properties (Ahola et al. 2008; Fujisawa et al. 2012).

W. Im · A. Rajabi Abhari · H. J. Youn · H. L. Lee (✉)
Department of Forest Sciences, College of Agriculture
and Life Sciences, Seoul National University, 1 Gwanak-
ro, Gwanak-gu, Seoul 08826, Korea
e-mail: lhakl@snu.ac.kr

The morphological properties of CNFs are essential parameters for controlling the mechanical properties of CNF-based materials. Microscopic techniques including SEM and TEM can accurately measure the diameter of the fibers (Iwamoto et al. 2014; Uetani and Yano, 2012; Pääkkö et al. 2007). Atomic force microscopes (AFM) have also been used to measure nanofibril length (Shinoda et al. 2012; Saito et al. 2013). The microscopic measurements must be made at different magnifications, as CNFs have broad fiber diameter distribution (Zhang et al. 2012). However, the length of the fibers cannot be readily obtained from microscopy images, as a CNF is too long to be observed in its entirety under high magnification (Ishii et al. 2011). Furthermore, the high aspect ratio fibers tend to become entangled with each other, which makes it difficult to determine the ends of a single fiber (Ishii, et al. 2011).

Fukuzumi et al. (2013) measured the length and length distribution of TEMPO-oxidized CNF (TOCN) using transmission electron microscope (TEM) images and investigated the effect of CNF length on film properties. They found that films prepared with a longer average length TOCN had high tensile strength and elongation at break. However, it was not easy to determine the fibril length using electron microscopes (TEM or SEM), even though these techniques offer clear and instant understanding of the structural features of CNF, because numerous observations are required for statistically reliable size evaluations.

To overcome the weaknesses of microscopic measurements, the average lengths of cellulose nanofibrils dispersed in water have been estimated using dynamic viscoelastic or shear viscosity measurements of CNF suspensions (Tanaka et al. 2014; Ishii et al. 2011). The average lengths determined by rheological measurement have been one order of magnitude higher than those measured by microscopy. This discrepancy has been attributed to the fact that the nanofibrils used in the dynamic viscoelastic measurements were not completely isolated, but partially aggregated in water (Tanaka et al. 2014).

Sedimentation experiments could also be used to assess the aspect ratio of CNFs. Raj et al. (2016) evaluated aspect ratios using the sedimentation method proposed by Zhang et al. (2012). Theoretically, the sedimentation method is based on a gel point (or critical concentration) that is defined as the lowest volume fraction where the fiber forms a continuous

network. Kerekes and Schell (1992) defined the crowding factor, N , as the number of fibers in a spherical volume with a diameter equal to the length of a fiber. The crowding factor can be expressed as follows:

$$N = (2/3)\Phi A^2, \quad (1)$$

where Φ and A are the volumetric concentration and aspect ratio of fiber, respectively. Experimentally, the gel point occurs at a crowding number of approximately $16(\pm 4)$, as proposed by Martinez et al. (2001). Then, volumetric concentration for the gel point, Φ_c , can be simplified as follows:

$$\Phi_c = 24/A^2. \quad (2)$$

For fiber suspension, it is often convenient to use weight fraction, C . According to Varanasi et al. (2013), C can be written as follows:

$$C = \rho_f \Phi / (\rho_f \Phi + \rho_l (1 - \Phi)), \quad (3)$$

where ρ_f and ρ_l are the density of the fibers and liquid, respectively. Thus, if $\Phi \ll 1$, then Eq. (3) may be re-expressed as follows:

$$\Phi_c = C_c (\rho_l / \rho_f), \quad (4)$$

where C_c is the weight fraction of the gel point. Then, combining Eqs. (2) and (4), the aspect ratio of the fiber can be calculated using the weight fraction of the gel point. The assumed density of the CNF is 1.5 g/cm^3 (Svagan et al. 2008; Varanasi et al. 2013).

Several studies have examined how the charge content of pulp fiber influences the mechanical energy that is required to completely isolate the pulp fiber (Tejado et al. 2012; Syverud et al. 2011). Besbes et al. (2011) found that pulp with higher carboxyl content reduced the mechanical energy consumption and that TOCN prepared with different levels of carboxyl content have almost homogeneous widths (3–4 nm), regardless of the mechanical treatment intensity.

The fundamental properties of CNF-based products are influenced by the CNF morphologies. However, the effect of the mechanical intensity and carboxyl content on the morphological properties of CNF has not been studied in detail. In this study, we investigated the effect of carboxyl content and mechanical intensity (i.e., number of grinding pass) on the morphological properties of carboxymethylated CNFs (CM CNFs). In addition, the effect of preparation

conditions on the rheological properties of CM CNF suspension and the mechanical properties of CM CNF film were investigated.

Experimental material

Never-dried bleached eucalyptus kraft pulp provided by Moorim P&P (Ulsan, Korea) was used as a starting raw material. The chemical composition of the pulp was evaluated according to TAPPI Method (T 203 om-93). The pulp consisted of $79.4 \pm 0.6\%$ cellulose, $18.8 \pm 0.2\%$ hemicelluloses, and small amounts of lignin and ash. Monochloroacetic acid (Sigma–Aldrich, 99.0%, MCA), sodium hydroxide (Samchun chemical, 98.0%), and isopropanol (Duksan Reagents, 99.5%, IPA) were used without further purification for the carboxymethylation.

Preparation of carboxymethylated CNF

The carboxymethylation reaction was carried out according to the method described by Im et al. (2018). Briefly, the pulp fiber was washed with deionized water and filtered by a vacuum filtration system to a consistency of 24% before carboxymethylation. Then, the pulp fiber was impregnated for 30 min at 35 °C with a solution of NaOH in IPA for alkalization. MCA dissolved in IPA was added to this reaction chamber for esterification, which was carried out for 60 min at 65 °C. The carboxyl content of the pulp fiber was controlled by changing the amounts of MCA (Table 1). The carboxyl content of the carboxymethylated pulp was determined using a conductometric titration method in accordance with SCAN-CM 65:02.

To produce CM CNFs, the consistency and total volume of the CM pulp suspension was adjusted to 0.5 wt% and 3 L, respectively. The pulp suspension was passed through a grinder (Super Masscolloider,

Masuko Sangyo Co., Ltd., Japan). The operation speed and gap distance were 1500 rpm and $-80 \mu\text{m}$, respectively.

Transmission electron microscopy (TEM, Carl Zeiss, LIBRA 120, Germany) was used to evaluate the width of the CM CNFs with different carboxyl contents. For TEM analysis, the CM CNF suspension was diluted with deionized water to 0.002% and then deposited on a glow-discharged carbon grid (Carbon type-B, Ted Pella Inc.). The CM CNF samples were observed at an accelerating voltage of 160 kV after negative staining. The average width of the CM CNFs was obtained using Image-J software. Furthermore, the cupriethylenediamine (CED) viscosity of the CM CNFs was measured to investigate the degree of polymerization according to the TAPPI Standard (T 230 om-08).

Estimation of the aspect ratios of CM CNFs

It is difficult to settle down the highly charged CNFs in water suspension because the repulsive forces make the charged CNFs stable (Iwamoto et al. 2014). Onyianta and Williams (2018) evaluated the gel point of carboxymethylated and TEMPO-oxidized CNFs by adding inorganic salts. In this study, the gel point analysis by sedimentation was employed to calculate the aspect ratios of the CM CNFs. To screen the surface charge before the sedimentation experiments, CM CNF samples with different carboxyl contents were diluted with deionized water to 0.3 wt%, and then dispersed in NaCl solutions with concentrations ranging from 0.03 to 0.18 M at 0.1 w/v%. The zeta potentials of the CNFs at different salt concentrations were evaluated using Zetasizer (Nano Zs, Malvern Instruments, Ltd.) at 25 °C. The sedimentation experiments were conducted with CM CNFs that had the same zeta potential, which was achieved by dispersing the CM CNF in salt solutions with different concentrations based on the carboxyl contents of the CM

Table 1 Reaction conditions for the carboxymethylation of pulp

Pulp fiber, g	Condition	Total volume of IPA, mL	NaOH, mmol/g dry pulp	MCA, mmol/g dry pulp
19	A	1800	3.68	0.96
	B			0.80
	C			0.50

CNFs. CM CNF suspensions with 0.1–0.02 w/v% consistency were prepared and allowed to fully sediment in 50 mL glass cylinders for 5 days. The plot of the concentration against the relative sediment height (sediment height H_s to initial suspension height H_0) was fitted with a quadratic equation, where the linear fit shows the gel point/connectivity threshold. The aspect ratio was then calculated using Eqs. (2) and (4).

Rheological properties of CM CNF

The rheological properties of the CM CNFs were studied using a Bohlin cone and plate rheometer (CVO, Malvern instrument, USA) with a gap angle between the cone and plate of 4° and a cone diameter of 4 cm. The rotational viscosity with an increase in shear rate was measured using CM CNF suspensions at 0.5 wt%. An oscillatory rheometer was also used to find the network properties of the CM CNF suspensions. Two modes of amplitude sweeps were carried out to evaluate the rheological properties of the CM CNFs. One shear-stress-amplitude sweep was performed in the range of 0.5–100 Pa at a constant frequency of 1 Hz and a second shear-strain-amplitude sweep was carried out in the range of 1–100 Hz at a constant stress of 0.5 Pa.

Preparation and analysis of CM CNF film

CM CNF films were prepared by pouring the CM CNF suspensions onto polystyrene petri dishes after degassing under a 0.1 MPa vacuum for 1 h and drying at 25°C and 55% humidity for 6 days. The mechanical properties of the CM CNF films, such as tensile property, elongation at break, and modulus of elasticity, were evaluated using a Universal Testing Machine (Instron Co., USA). The width of the specimen and the measurement span were 15 and 30 mm, respectively. The strain rate during measurement was 3 mm/min. The crystallinity of the CM CNF films was measured using an X-ray diffractometer with a Cu K α X-ray source (XRD, Bruker, D8 Advance, Germany) set at 5–40 degrees with a scanning speed of 0.5 s/step. The crystallinity index was estimated from the diffraction patterns using the Segal method. The crystallinity was calculated from the height ratio between the intensity of the crystalline peak ($I_{200} - I_{AM}$) and total intensity (I_{200}) according to Eq. (5).

$$\text{Crystallinity}(\%) = ((I_{200} - I_{AM}) / I_{200}) \times 100, \quad (5)$$

where I_{200} is the total intensity of the 200 peak at $2\theta = 22.7^\circ$, and I_{AM} is the minimum intensity between the 200 and 110 peaks at $2\theta = 18^\circ$, respectively (Thygesen et al. 2005).

Results and discussion

Characteristics of the CM pulp and CNFs

Table 2 shows the characteristics of the CM pulp and CNFs manufactured under the different reaction conditions. The carboxyl content of the pulp fiber increased as the amount of MCA increased. The number of grinding passes required to obtain completely isolated CM CNFs decreased as the carboxyl content increased, which is consistent with previous studies by Tejado et al. (2012) and Wågberg et al. (2008). The average widths of the three CM CNF samples were similar, ranging from 4.9 to 5.1 nm, as shown in Table 2. Figure 1 also shows that the shapes of the CM CNFs were very similar. However, the CED viscosity value, which indicates the degree of polymerization of cellulose, decreased as the number of grinding passes increased. Shinoda et al. (2012) investigated the relationship between the length and degree of polymerization (DP) of TOCNs and concluded that there is a linear relationship between the average fibril length and the DP of TOCNs. This implies that a reduction in CED viscosity accompanied by an increase in the number of grinding passes is associated with the reduction of the CM CNF length.

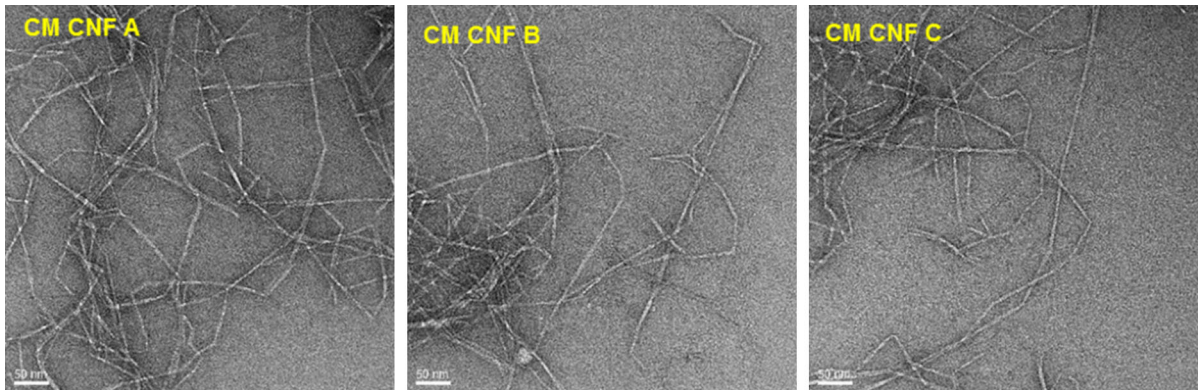
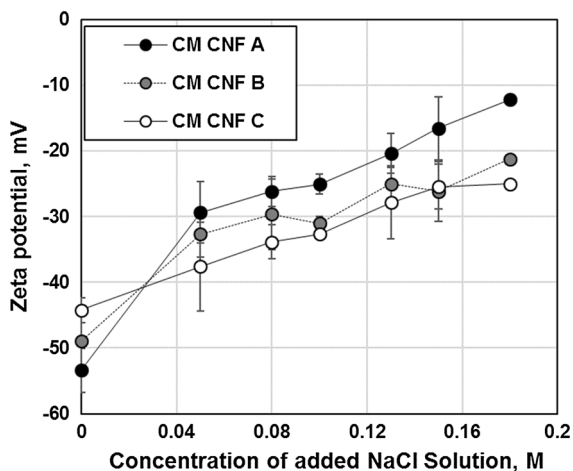
Aspect ratios of CM CNFs manufactured under different conditions

It is difficult to determine the ends of a single fiber in TEM images because many fibrils are entangled with each other and the image areas are not large enough to display whole fibrils from end to end (Fig. 1). This problem associated with the microscopic analysis in the CNF length measurement can be resolved using a sedimentation experiment.

Before carrying out the sedimentation experiment, the zeta-potential of the CM CNFs at 0.1 w/v% was determined using NaCl concentration (Fig. 2). CM CNF A, which had the highest carboxyl content,

Table 2 Characteristics of CM CNFs produced under different reaction conditions

Classification	Carboxyl contents, $\mu\text{mol/g}$	The number of grinding pass	Width, nm (st.dev)	CED viscosity, mPa s
CM CNF A	510	4	5.1 (0.98)	6.57
CM CNF B	330	7	5.1 (1.05)	6.26
CM CNF C	220	10	4.9 (0.87)	4.98

**Fig. 1** TEM images of the CM CNFs with different carboxyl content and number of grinding passes**Fig. 2** Zeta potential of CM CNFs at different salt concentration

showed a zeta-potential of -53 mV in deionized water, because it had more carboxyl groups than CM CNF B and C. Increases in the NaCl concentration led to more rapid changes in the zeta potential of CM CNF A. The zeta potentials of CM CNF B and C also changed with the increase in salt concentration. CM CNF C, which had the lowest carboxyl content, had the smallest change in zeta potential with salt

concentration. The zeta potentials of the three CM CNF samples were adjusted to -25 mV, which was the zeta potential of untreated CNF, by adjusting the concentrations of salt solutions. The zeta potentials of -25 mV for CM CNF A, CM CNF B, and CM CNF C were obtained by adjusting the concentration of salt solutions to 0.1, 0.13, and 0.18 M, respectively. These salt concentrations were used to dilute the three CM CNF samples to 0.2–1.0 w/v% for the sedimentation experiments.

Figure 3 shows the quadratic fit of the plot of the concentration of CM CNFs against the relative sediment height. Table 3 displays the results of the sedimentation experiment including the quadratic regression, gel point, and calculated aspect ratio. The width, zeta potential, and length of the CM CNFs might influence the sedimentation tendency. The width and zeta potential of the three CM CNFs were very similar to each other. Therefore, the aspect ratio is the only one of the three factors that affects sedimentation tendency. Table 3 shows that the CM CNFs prepared under different conditions had different aspect ratios. CM CNF A, which had the highest carboxyl content and underwent the mildest mechanical treatment, had the highest aspect ratio of 171. This

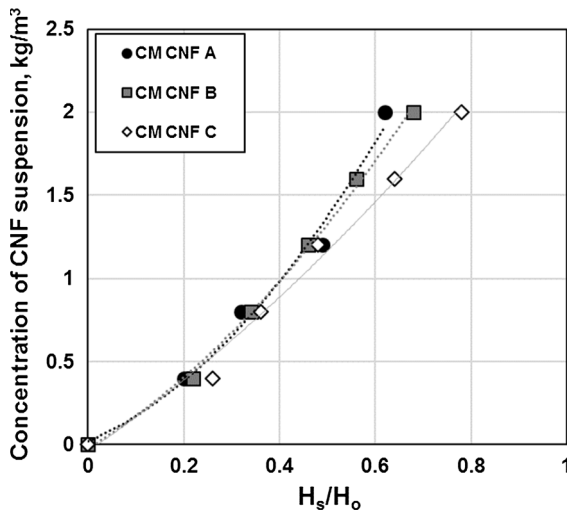


Fig. 3 Sedimentation tendency of CM CNFs

indicates that the carboxyl content of CM CNFs influences both the mechanical energy needed to produce the CNF and the aspect ratio of the fibrils. Wågberg et al. (2008) reported that the length (L) and width (d) of CM CNF was $L \leq 1 \mu\text{m}$ and $d \approx 5\text{--}15 \text{ nm}$, respectively. This result agrees with the results calculated from sedimentation. Onyianta and Williams (2018) also calculated the aspect ratio of charged CNF using sedimentation. It was reported that the aspect ratio of CM CNF with carboxyl content of $550 \mu\text{mol/g}$ was 229 ± 18 . This difference was likely attributed to different salt concentration to dilute CNF, which influenced charge properties of CNF.

Rheological properties of CM CNF

Figure 4 shows the rheological properties of the CM CNFs at 0.5 wt%. Shear thinning was clearly observed (Fig. 4a), which was caused by the interactions between fibrils orientated along the shear direction. CM CNF A had a higher shear viscosity than the other two CNFs. The shear viscosities of CM CNF B and C

were the same, irrespective of the carboxyl content and mechanical treatment level. The amplitude and frequency sweep mode measurements were performed to find the network properties of the CM CNFs. Figure 4(b) plots the storage modulus of CM CNFs against shear stress. The storage modulus had a plateau region in the low shear stress range. When the shear stress increased beyond the yield stress, the storage modulus decreased significantly. Yield stress is generally accepted as an indication of network strength. The network associated with the fibrils began to break down at the yield point. In a CNF system, yield stress depends on the aspect ratio (Müller et al. 2017; Li et al. 2015). Obviously, CM CNF A had a higher yield stress than CNF-B and CNF-C (CNF-A:47 Pa, CNF-B:33 Pa, CNF-C:26 Pa), which is consistent with CM CNF A's high aspect ratio, as measured in the sedimentation experiment. Onyianta et al. (2018) also evaluated the aspect ratio and rheological properties of TEMPO-oxidized CNF and CM CNF. They concluded that the CNF with higher aspect ratio showed higher storage modulus and critical strain. Figure 4c shows the storage modulus as a function of frequency. The storage modulus increased as the aspect ratio increased, indicating that the CM CNF with the highest aspect ratio had the strongest network properties.

Mechanical properties of CM CNF film

Figure 5 and Table 4 show the XRD patterns and crystallinities of CNF samples, respectively. The crystallinities of the three CM CNF samples were around 60%, suggesting that carboxymethylation and mechanical treatment had no significant effects on crystallinity. Similar results have been reported by Siró et al. (2010) and Aulin et al. (2009). The densities of the CM CNFs films prepared using three CNFs are also listed in Table 4. The density of the film made of CM CNF C was higher than those of two other films,

Table 3 Quadratic regression, gel point, and aspect ratio

Classification	Quadratic regression (R^2)	Gel point (weight fraction)	Aspect ratio
CM CNF A	$y = 2.95x^2 + 1.227 \times (0.988)$	0.0012	171
CM CNF B	$y = 1.85x^2 + 1.767 \times (0.997)$	0.0018	142
CM CNF C	$y = 0.91x^2 + 1.952 \times (0.989)$	0.0020	135

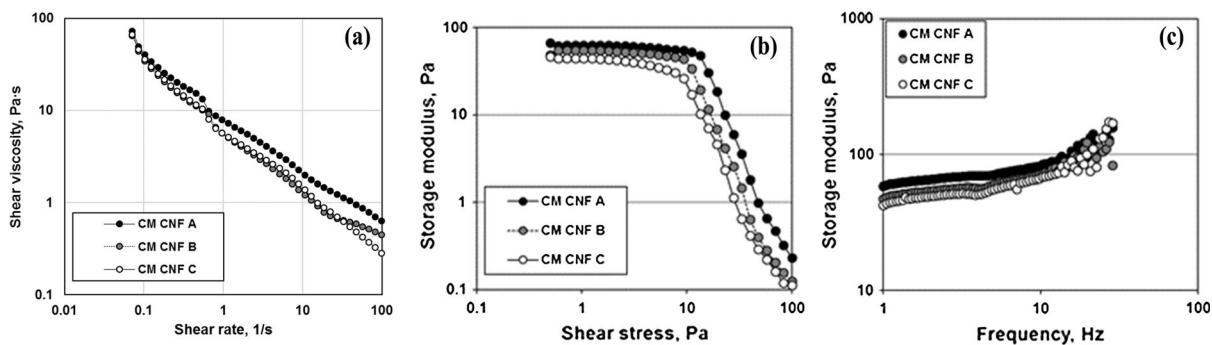


Fig. 4 Rheological properties of the CM CNFs: **a** shear viscosity, **b** the storage modulus as a function of stress, and **c** the storage modulus with frequency sweep

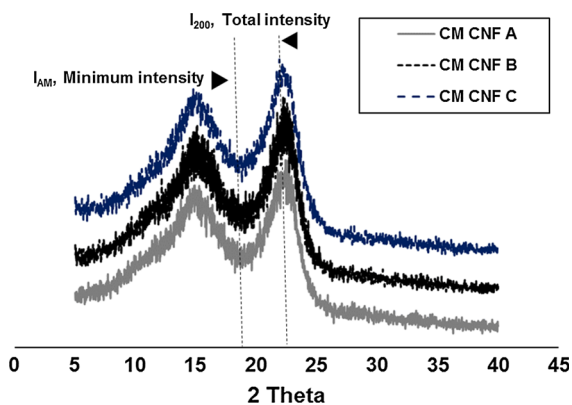


Fig. 5 The XRD pattern of CM CNFs

Table 4 Properties of the CM CNF films

Sample	Crystallinity, %	Density, g/cm ³
CM CNF A	60.4	1.03
CM CNF B	64.8	1.04
CM CNF C	58.6	1.19

presumably because of its low aspect ratio as mentioned by Zhao et al. (2015).

Figure 6 shows the mechanical properties of the CM CNF films. There are clear correlations between the morphological properties of the CNF and the mechanical properties of the CNF films. There was a linear relationship between the tensile index and tensile strength of CNFs (Fig. 6a). This indicated that the tensile property of film at the same basis weight is proportional to the aspect ratio. The film produced using CM CNF with a high aspect ratio also showed a

high elongation at the break but a low modulus of elasticity due to the interconnection between fibrils. Fukuzumi et al. (2013) have shown that an increase in fibril length improves tensile strength and elongation at break. Lower tensile index of CM CNF film was attained compare with the results by Naderi et al. (2015). And this was attributed to the fact that the grinder gave lower specific area of CNF than homogenizer as pointed out by Spence et al. (2011).

Conclusions

The influence of carboxyl content and mechanical treatment on the morphological properties of CM CNF was investigated. The carboxyl content of the pulp fiber was controlled by controlling the amount of MCA in the carboxymethylation reaction. The network properties of CM CNF suspensions and the mechanical properties of CM CNF films were also evaluated. The width was measured using TEM image analysis and the aspect ratio of the CM CNF was investigated using sedimentation experiments. To settle down the fibrils under the same condition, the zeta potential of the CM CNFs with different carboxyl content was controlled by adding salt solutions. The aspect ratio was decreased as the number of grinding passes increased, which was dependent on the carboxyl content of the pulp fiber. The CM CNF with the highest aspect ratio had the greatest network strength in suspension and produced the film with the strongest mechanical properties.

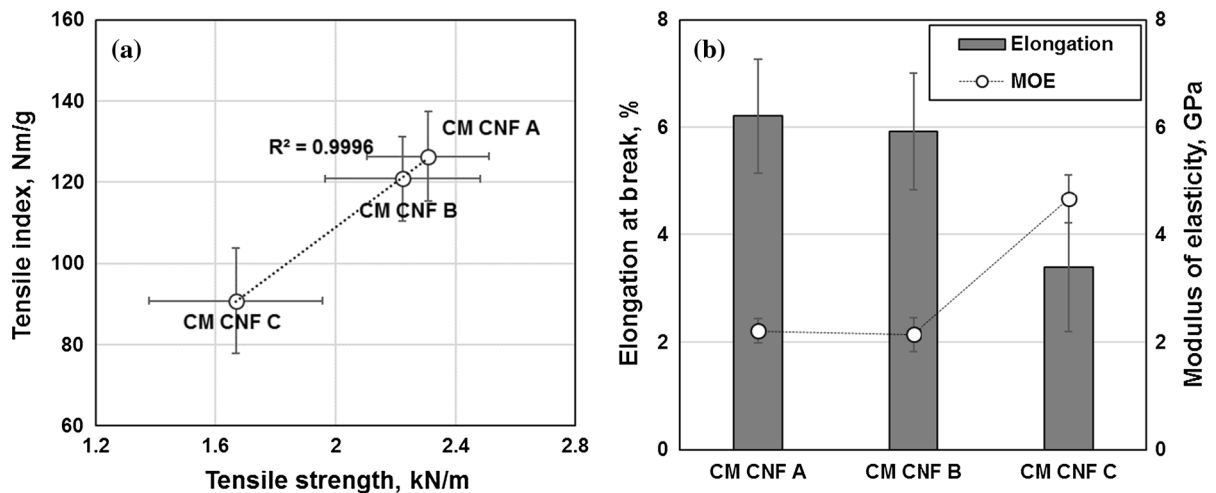


Fig. 6 Mechanical properties of the CM CNF films: **a** relationship between tensile index and tensile strength of CNFs films, **b** elongation at break and modulus of elasticity for three CNFs

Acknowledgments This work was supported by the Technological Innovation Program funded by the Ministry of Trade, Industry & Energy (10062717).

References

- Ahola S, Salmi J, Johansson LS, Laine J, Österberg M (2008) Model films from native cellulose nanofibrils. Preparation, swelling, and surface interactions. *Biomacromolecules* 9:1273–1282. <https://doi.org/10.1021/bm701317k>
- Aulin C, Ahola S, Josefsson P, Nishino T, Hirose Y, Österberg M, Wågberg L (2009) Nanoscale cellulose films with different crystallinities and mesostructured-their surface properties and interaction with water 25(13):7675–7685. <https://doi.org/10.1021/la900323n>
- Besbes I, Alila S, Boufi S (2011) Nanofibrillated cellulose from TEMPO-oxidized eucalyptus fibres: effect of the carboxyl content. *Carbohydr Polym* 84:975–983. <https://doi.org/10.1016/j.carbpol.2010.12.052>
- Errezma M, Mabrouk AB, Boufi S (2017) Waterborne acrylic-cellulose nanofibrils nanocomposite latexes via miniemulsion polymerization. *Prog Org Coat* 109:30–37. <https://doi.org/10.1016/j.porgcoat.2017.04.003>
- Fujisawa S, Ikeuchi T, Takeuchi M, Satio T, Isogai A (2012) Superior reinforcement effect of TEMPO-oxidized cellulose nanofibrils in polystyrene matrix: optical, thermal, and mechanical studies. *Biomacromolecules* 13:2188–2194. <https://doi.org/10.1021/bm300609c>
- Fujisawa S, Saito T, Kimura S, Iwata T, Isogai A (2013) Surface engineering of ultrafine cellulose nanofibrils toward polymer nanocomposite materials. *Biomacromolecules* 14:1541–1546. <https://doi.org/10.1021/bm400178m>
- Fukuzumi H, Saito T, Isogai A (2013) Influence of TEMPO-oxidized cellulose nanofibril length on film properties. *Carbohydr Polym* 93:172–177. <https://doi.org/10.1016/j.carbpol.2012.04.069>
- Im WH, Lee S, Abhari AR, Youn HJ, Lee HL (2018) Carboxymethylation as a pretreatment for low cost production of cellulose nanofibrils. *Cellulose* 25:3873–3883. <https://doi.org/10.1007/s10570-018-1853-9>
- Ishii D, Saito T, Isogai A (2011) Viscoelastic evaluation of average length of cellulose nanofibers prepared by TEMPO-mediated oxidation. *Biomacromol* 12:548–550. <https://doi.org/10.1021/bm1013876>
- Isogai A (2018) Present situation and future prospects of nanocellulose R&D in Japan. In: 2018 TAPPI international conference on nanotechnology for renewable materials, TAPPI
- Iwamoto S, Lee SH, Endo T (2014) Relationship between aspect ratio and suspension viscosity of wood cellulose nanofibers. *Polym J* 46:73–76. <https://doi.org/10.1038/pj.2013.64>
- Kerekes RJ, Schell CJ (1992) Characterization of fibre flocculation regimes by a crowding factor. *J Pulp Pap Sci* 18(1):J32–J38
- Ko CH, Chen FJ, Lee JJ, Tzou DLM (2011) Effects of fiber physical and chemical characteristics on the interaction between endoglucanase and eucalypt fibers. *Cellulose* 18:1043–1054. <https://doi.org/10.1007/s10570-011-9534-y>
- Li MC, We Q, Song K, Qing Y, We Y (2015) Cellulose nanoparticles as modifiers for rheology and fluid loss in bentonite water-based fluids. *ACS Appl Mater Interfaces* 7:5006–5016. <https://doi.org/10.1021/acsami.5b00498>
- Liu D, Sun X, Tian H, Maiti S, Ma Z (2013) Effects of cellulose nanofibrils on the structure and properties on PVA nanocomposites. *Cellulose* 20(6):2981–2989. <https://doi.org/10.1007/s10570-013-0073-6>
- Martinez DM, Buckley K, Jivan S, Lindström A, Triruvengadaswamy R, Olson JA, Ruth TJ, Kerekes RJ (2001) Characterizing the mobility of papermaking fibres during sedimentation. In: 12th fundamental research symposium, Oxford, pp 225–254
- Müller M, Öztürk E, Arlov Ø, Gatenholm P, Wong MZ (2017) Alginate sulfate-nanocellulose bioinks for cartilage

- bioprinting applications. *Ann Biomed Eng* 1:210–223. <https://doi.org/10.1007/s10439-016-1704-5>
- Naderi A, Lindström T, Sundström J (2015) Repeated homogenization, a route for decreasing the energy consumption in the manufacturing process of carboxymethylated nanofibrillated cellulose? *Cellulose* 22:1147–1157. <https://doi.org/10.1007/s10570-015-0576-4>
- Nechyporchuk O, Belgacem MN, Bras J (2016) Production of cellulose nanofibrils: a review of recent advances. *Ind Crops Prod* 93:2–25. <https://doi.org/10.1016/j.indcrop.2016.02.016>
- Onyianta AJ, Williams R (2018) The use of sedimentation for the estimation of aspect ratios of charged cellulose nanofibrils. In: Fangueiro R, Rana S (eds) *Advances in Natural Fibre Composites*. Springer, Cham, pp 195–203
- Onyianta AJ, Dorris M, Williams RL (2018) Aqueous morpholine pre-treatment in cellulose nanofibril(CNF) production: comparison with carboxymethylation and TEMPO oxidation pre-treatment methods. *Cellulose* 25:1047–1064. <https://doi.org/10.1007/s10570-017-1631-0>
- Pääkkö M, Ankerfors M, Kosonen H, Nykänen A, Ahola S, Österberg M, Ruokolainen J, Laine J, Larsson PT, Ikkala O, Lindström T (2007) Enzymatic hydrolysis combined with mechanical shearing and high-pressure homogenization for nanoscale cellulose fibrils and strong gels. *Biomacromolecules* 8:1934–1941
- Raj P, Mayahi A, Lahtinen P, Varanasi S, Garnier G, Martin D, Batchelor W (2016) Gel pint as a measure of cellulose nanofibre quality and feedstock development with mechanical energy. *Cellulose* 23:3051–3064. <https://doi.org/10.1007/s10570-016-1039-2>
- Saito T, Okita Y, Nge TT, Sugiyama J, Isogai A (2006) TEMPO-mediated oxidation of native cellulose: microscopic analysis of fibrous fractions in the oxidized products. *Carbohydr Polym* 65:435–440. <https://doi.org/10.1016/j.carbpol.2006.01.034>
- Saito T, Kuramae R, Wohlerl J, Berglund LA, Isogai A (2013) An ultrastrong nanofibrillar biomaterial: the strength of single cellulose nanofibrils revealed via sonication-induced fragmentation. *Biomacromolecules* 14:248–253. <https://doi.org/10.1021/bm301674e>
- Shinoda R, Saito T, Okita Y, Isogai A (2012) Relationship between length and degree of polymerization of TEMPO-oxidized cellulose nanofibrils. *Biomacromolecules* 13:842–849. <https://doi.org/10.1021/bm2017542>
- Siró I, Plackett D, Hedenqvist M, Ankerfors M, Lindström T (2010) Highly transparent films from carboxymethylated microfibrillated cellulose: the effect of multiple homogenization steps on key properties. *J Appl Polym Sci* 116(5):2652–2660. <https://doi.org/10.1002/app.32831>
- Spence KL, Venditti RA, Rojas OJ, Habibi Y, Pawlak JJ (2011) A comparative study of energy consumption and physical properties of microfibrillated cellulose produced by different processing methods. *Cellulose* 18:1097–1111. <https://doi.org/10.1007/s10570-011-9533-z>
- Suflet DM, Chitanu GC, Popa VI (2006) Phosphorylation of polysaccharides: new results on synthesis and characterization of phosphorylated cellulose. *React Funct Polym* 66:1240–1249. <https://doi.org/10.1016/j.reactfunctpolym.2006.03.006>
- Svagan AJ, Azizi Samir MAS, Berglund LA (2008) Biomimetic foams of high mechanical performance based on nanostructured cell wall reinforced by native cellulose nanofibrils. *Adv Mater* 20:1263–1269. <https://doi.org/10.1002/adma.200701215>
- Syverud L, Carrasco GC, Toledo J, Toledo PG (2011) A comparative study of eucalyptus and pinus radiata pulp fibres as raw materials for production of cellulose nanofibrils. *Carbohydr Polym* 84:1033–1038. <https://doi.org/10.1016/j.carbpol.2010.12.066>
- Tanaka R, Saito T, Ishii D, Isogai A (2014) Determination of nanocellulose fibril length by shear viscosity measurement. *Cellulose* 21:1581–1589. <https://doi.org/10.1007/s10570-014-0196-4>
- Tejado A, Alam MN, Antal M, Yang H, van de Ven TGM (2012) Energy requirements for the disintegration of cellulose fibers into cellulose nanofibers. *Cellulose* 19:831–842. <https://doi.org/10.1007/s10570-012-9694-4>
- Thygesen A, Oddershede J, Lilholt H, Thomsen AB, Ståhl K (2005) On the determination of crystallinity and cellulose content in plant fibres. *Cellulose* 12:563–576. <https://doi.org/10.1007/s10570-005-9001-8>
- Uetani K, Yano H (2012) Zeta potential time dependence reveals the swelling dynamics of wood cellulose nanofibrils. *Langmuir* 28:818–827. <https://doi.org/10.1021/la203404g>
- Varanasi S, He R, Batchelor W (2013) Estimation of cellulose nanofibre aspect ratio from measurements of fibre suspension gel point. *Cellulose* 20:1885–1896. <https://doi.org/10.1007/s10570-013-9972-9>
- Wågberg L, Decher G, Norgren M, Lindström T, Ankerfors M, Axnäs K (2008) The build-up of polyelectrolyte multilayers of microfibrillated cellulose and cationic polyelectrolytes. *Langmuir* 24(3):784–795. <https://doi.org/10.1021/1a70248v>
- Wang W, Sabo RC, Mozuch MD, Kersten P (2015) Physical and mechanical properties of cellulose nanofibril films from bleached eucalyptus pulp by endoglucanase treatment and microfluidization. *J Polm Environ* 23:551–558. <https://doi.org/10.1007/s10924-015-0726-7>
- Yao K, Huang S, Tang H, Xu Y, Buntkowsky G, Berglund LA, Zhou Q (2017) Bioinspired interface engineering for moisture resistance in nacre-mimetic cellulose nanofibrils/clay nanocomposite. *ACS Appl Mater Interfaces* 9:20169–20178. <https://doi.org/10.1021/acsami.7b02177>
- Zhang L, Batchelor W, Varanasi S, Tsuzuki T, Wang X (2012) Effect of cellulose nanofiber dimensions on sheet forming through filtration. *Cellulose* 19:561–574. <https://doi.org/10.1007/s10570-011-9641-9>
- Zhao Y, Xu C, Xing C, Shi X, Matuana LM, Zhou H, Ma X (2015) Fabrication and characteristics of cellulose nanofibrils films from coconut palm petiole prepared by different mechanical processing. *Ind Crops Product* 65:96–101. <https://doi.org/10.1016/j.indcrop.2014.11.057>